Renewable Energy 139 (2019) 1391–1399

Contents lists available at ScienceDirect

Renewable Energy

journal homepage: www.elsevier.com/locate/renene

Hydrodeoxygenation of oleic acid and palmitic acid to hydrocarbon-like biofuel over unsupported Ni-Mo and Co-Mo sulfide catalysts

Boonyawan Yoosuk [a, **], Paphawee Sanggam [b], Sakdipat Wiengket [c], Pattarapan Prasassarakich [c, d, *]

[a] Renewable Energy Laboratory, National Metal and Materials Technology Center (MTEC), National Science and Technology Development Agency Pathum Thani, 12120, Thailand
[b] Program in Petrochemistry and Polymer Science, Faculty of Science, Chulalongkorn University, Bangkok 10330, Thailand
[c] Department of Chemical Technology, Faculty of Science, Chulalongkorn University, Bangkok 10330, Thailand
[d] Center for Petroleum, Petrochemicals and Advanced Materials, Chulalongkorn University, Bangkok 10330, Thailand

ARTICLE INFO

Article history:
Received 24 April 2018
Received in revised form
16 January 2019
Accepted 6 March 2019
Available online 9 March 2019

Keywords:
Hydrodeoxygenation
Bio-hydrogenated diesel
Oleic acid
Palmitic acid
Sulfide catalysts

ABSTRACT

Second generation biodiesel, so-called bio-hydrogenated diesel (BHD), can be produced from hydrotreatment of vegetable oils. The hydrogenation (HDO) of oleic acid and palmitic acid as model compounds of palm oil over unsupported Ni-Mo and Co-Mo sulfide catalysts was performed in a Parr reactor to produce BHD. The effects of reaction parameters: temperature, hydrogen pressure and the atomic ratio of catalysts (Ni/(Ni + Mo) or Co/(Co + Mo)) on the conversion and product yields (mainly n-C_{15}, n-C_{16}, n-C_{17} and n-C_{18} hydrocarbons) were evaluated. The results show that the high pressure favored HDO pathway, while high temperature strongly affected the decarboxylation and decarbonylation pathways. At optimal conditions for oleic acid HDO, the efficient catalyst was $NiMoS_2$ catalyst (Ni/(Ni + Mo) = 0.2) which gave high oleic acid conversion (100%), n-C_{18} selectivity (78.8%) and n-C_{18} yield (70.3%) whereas, for palmitic acid HDO, $NiMoS_2$ catalyst (Ni/(Ni + Mo) = 0.2) also gave high palmitic acid conversion (95.2%), n-C_{16} selectivity (78.5%) and n-C_{16} yield (65.6%).

1. Introduction

The conventional method of biodiesel production is the transesterification of oil (triglycerides) with methanol or ethanol to produce fatty acid methyl or ethyl esters (FAME or FAEE, respectively), which is called first generation biodiesel. However, FAME and FAEE have a low oxidation resistance, low compatibility with diesel and the presence of some glycerol by-products as their limitations. Nowadays, the research on the production of hydrogenated vegetable oil has been focused as it is second biodiesel generation [1]. The bio-hydrogenated diesel (BHD) is becoming more attractive for utilization as renewable energy source for diesel engines. In the BHD approach, triglyceride molecules in oil react with H_2 gas and form hydrocarbons, mostly normal alkanes, via hydrodeoxygenation (HDO), decarbonylation and decarboxylation at high reaction temperature (300–360 °C) and hydrogen (H_2) pressure above 3 MPa [2]. Typically, propane, carbon dioxide and water are found as by-products. The main advantages are the higher heating value and cetane number compared to that for FAME [1,3].

In some countries, such as Thailand, palm oil is the highest potential feedstock for biodiesel production. However, with the ethics of the conflict over the use of agricultural land for food vs. fuel production, many researchers are turning their focus to utilize inedible or waste oil. In order to render the oils to an edible form, the impurities as gum (phospholipids and phosphatides) are removed. Firstly, the degummed palm oil was obtained by precipitation, then the pigments, trace metals and other undesirable impurities were removed by using bleaching earth, thereafter deodorization step was applied. The result is the refined, bleached,

* Corresponding author. Department of Chemical Technology, Faculty of Science, Chulalongkorn University, Bangkok 10330, Thailand.
** Corresponding author.
E-mail addresses: boonyawy@mtec.or.th (B. Yoosuk), ppattara@chula.ac.th (P. Prasassarakich).

https://doi.org/10.1016/j.renene.2019.03.030
0960-1481/

deodorized (RBD) palm oil with the palm fatty acid distillate as a byproduct. Finally, the RBD palm oil is fractionated to yield refined palm olein and stearin, which are used as the raw materials to produce BHD.

There is increasing interest in the hydrotreatment process of RBD palm oil using various catalysts to produce BHD. Nickel-molybdenum NiMo/alumina (Al_2O_3) and cobalt-molybdenum CoMo/Al_2O_3 were recently employed as catalysts for BHD production. The catalysts are normally activated by the addition of a sulfur compound to give the sulphidation catalyst form. It is noteworthy that NiMo/Al_2O_3 and CoMo/Al_2O_3 have previously been employed as hydrodesulfurization (HDS) catalysts successfully. However, some researchers found that bimetallic carbide catalysts showed higher activities in the hydrodenitrogenation (HDN) and HDS reactions than the commercial NiMo/Al_2O_3 and Co-Mo/Al_2O_3 catalysts [4–6].

Recently, the hydroprocessing of soybean, sunflower, palm oil and cottonseed oils using different types of supported catalyst, i.e. hydrogenating catalysts (NiMo and CoMo) and noble metals (Pt, Pd, Ni and Ru) were explored for their potential in catalyzing alkane production [7–10]. For the hydrogenation of soybean oil using Pd or Ni catalyst, the n-paraffin content (n-C_{17} and n-C_{15}) was higher than 80% by weight (wt%), while the CoMo catalyst yielded isomerized and lighter hydrocarbons with less than 55 wt% n-paraffin [7]. Thus, NiMo or CoMo catalyst favored hydrodeoxygenation, while using the Pd catalyst, the main reaction pathway was decarboxylation. In the same manner, for hydrogenation of waste cooking oil over sulfide catalysts (NiMo, CoMo and NiW), the NiMo and NiW catalysts exhibited a high activity whereas decreasing activity was observed in the case of the CoMo catalyst [11].

While most research have been focused on Ni or Co promoted Mo or W based catalysts on Al_2O_3 support, a new generation of catalyst containing highly loaded or bulk metal sulfide (unsupported) emerged on the market (NEBULA-type catalysts) [12]. This type of catalyst has high active site density per catalyst weight which exhibits much higher activity than conventional catalysts. Thus, a synthesized technique of the new unsupported highly metal loaded sulfide catalysts is a promising research. The present work, unsupported Ni-Mo and Co-Mo sulfides were prepared by one step hydrothermal method. With this method, the unsupported catalyst is sulfided in one synthesized step. An additional sulfidation step is not required. It has been reported that highly active nano-sized Mo-based sulfide could be obtained from this hydrothermal method with water, organic solvent and hydrogen [13].

Palm oil consists of palmitic acid (40.8%) and oleic acid (45.2%) as the main components with lesser amounts of stearic acid (3.6%) and is considered a good feedstock for hydrocarbon-like biofuel production [14]. This study presents the information on the hydrodeoxygenation of palmitic acid and oleic acid as a model oil to produce hydrocarbon-like biofuel using unsupported Ni-Mo and Co-Mo sulfide catalysts. Ni or Co addition influences the properties and activity of amorphous unsupported Mo sulfide and the possibility of using this catalyst for palm oil hydrodeoxygenation is reported. The study of unsupported sulfide catalyst is a promising route for developing a better understanding and contributes to the development of better hydrogenation catalysts. The study on oleic acid and palmitic acid hydrodeoxygenation has allowed determining the effect of Ni addition on activity of unsupported Mo sulfide and its influence on the pathways. The present study provides insight into structure-activity-selectivity relationship and allows for controlling the catalyst selectivity as well as activity of unsupported Ni-Mo sulfide catalysts by tailoring amount of Ni or Co loading.

2. Experimental

2.1. Materials

Ammonium tetrathiomolybdate (ATTM; $(NH_4)_2MoS_4$, Sigma-Aldrich), oleic acid (Sigma-Aldrich), palmitic acid (Sigma-Aldrich), n-decane (Sigma-Aldrich), decahydronaphthalene (decalin, Fluka), nickel nitrate hexahydrate ($Ni(NO_3)_2 \cdot 6H_2O$, Sigma-Aldrich) and cobalt nitrate hexahydrate ($Co(NO_3)_2 \cdot 6H_2O$, Sigma-Aldrich) were used without further purification. To minimize an oxidative degradation of ATTM in long-time use, newly purchased reagent was kept in a refrigerator. The ATTM degradation may cause a deviation of activity of prepared MoS_2. Crystalline MoS_2 (commercial grade) powder (Sigma-Aldrich) was used for characterization as a reference for comparison.

2.2. Catalyst preparation

The Ni-Mo or Co-Mo sulfide catalysts were prepared using a hydrothermal method [15] in a 250-mL Parr reactor. ATTM (0.15 g dissolved in 25 g of deionized water) was mixed with the desired amount of $Ni(NO_3)_2 \cdot 6H_2O$ or $Co(NO_3)_2 \cdot 6H_2O$ (dissolved in the minimum amount of water) so as to give the atomic ratio of Ni/(Mo + Ni) or Co/(Co + Mo) of 0.1, 0.2, 0.3 or 0.4. Then, 2.5 g of organic solvent (decalin) was added. After that, the reactor was pressurized with H_2 to an initial pressure of 28 bar and heated to 350 °C for 60 min. The synthesized catalysts were separated by filtration technique and kept under an organic solvent. Each catalyst was designated as 'X-$NiMoS_2$' or 'X-$CoMoS_2$' where X represents the atomic ratio of Ni/(Ni + Mo) or Co/(Co + Mo).

The amorphous Mo sulfide catalyst (MoS_2-A) was prepared by the same procedure as for the Co(Ni)–Mo sulfide catalysts, but without the Co or Ni precursor. For Ni sulfide catalyst (Ni-S) or Co sulfide catalyst (Co-S), the same procedure was followed without the addition ATTM except CS_2 used as the sulfur source. Crystalline MoS_2 (MoS_2-C) powder purchased from Sigma-Aldrich was used as received.

2.3. Characterization of catalysts

The surface morphology of catalysts was examined by transmission electron microscopy (TEM) using a FEI-TECNAI G^2 S-Twin transmission electron microscope. A grinded sample was suspended in ethanol by using ultrasonic bath and the suspension was dropped on a microgrid carbon film supported by a Cu grid. The X-ray diffraction patterns were obtained on a X-ray diffractometer/Bruker AXS-D8 Discover with Cu K α emission, 40 mA 40 kV with a scanning speed of 0.02°/min.

The N_2 adsorption and desorption isotherms were measured on a Micromeritics ASAP 2064/ASAP 2060 instrument. Pore size distributions of the sample were determined from the isotherms by the Barrett-Joynor-Hallenda (BJH). Fresh catalyst samples were vacuum dried before the adsorption measurement. Temperature programmed reduction (TPR) of catalysts was conducted with a BELCAT-B instrument. The sample was heated up to 500 °C, held for 30 min and then cooled to room temperature under Ar flow. With introducing a mixture of 4.8 vol% H_2/Ar, the sample was again heated to 650 °C and the effluent gas was analyzed using thermal conductivity detector.

2.4. Hydrogenation (HDO) reaction

For hydrogenation of oleic acid or palmitic acid, the acid (0.3 g), decane (19.7 g) and catalyst (0.075 g or 0.375 wt% based on solution) were charged into a 250-mL Parr reactor which was then

pressurized with H_2 to the desired pressure. The reaction system was heated to the desired temperature and let to proceed for 4 h for oleic acid HDO (2 h for palmitic acid HDO) with constant stirring at 150 rpm. The reactor was then cooled to room temperature, the gas was released, and the reaction mixture was removed. The catalyst was recovered by vacuum filtration. The liquid products were quantitatively analyzed using gas chromatography (GC) with a flame ionization detector (FID; Shimadzu GC2010) equipped with a DB-1 column (60 m × 0.25 mm x 0.1 μm). The GC-FID was programmed from 50 °C to 250 °C at a heating rate of 5 °C/min. For the results of conversion and product yields, the average of two HDO experiments was considered as the representative value with narrow SD.

3. Results

3.1. HDO of oleic acid and palmitic acid

Hydrotreatment, including hydrogenation, of oleic acid and palmitic acid is very complex, which are influenced by the operating parameters, including the temperature, pressure and Ni/(Ni + Mo) or Co/(Co + Mo) atomic ratio. For hydrogenation over sulfide catalysts, it has been proposed that oleic acid and palmitic acid react with H_2 through hydrodeoxygenation (HDO), decarbonylation (DCO) and decarboxylation (DCO_2), as shown in Scheme 1.

3.1.1. Effect of temperature and pressure

The effect of reaction temperature on oleic acid HDO over 0.2-$NiMoS_2$ catalyst is presented in Table 1. The oleic acid conversion significantly increased with increasing reaction temperature and the C_{17} and C_{18} yields showed noticeable temperature dependence [16]. At a constant pressure of 60 bar, increasing hydrogenation temperature from 250 to 280 °C increased the oleic acid conversion from 87.4% to 100%. The increasing conversion with reaction temperature indicated that the HDO reaction was affected by reaction kinetics. As the temperature was increased, the oleic acid molecule gained more kinetic energy in exceeding activation energy to interact with H_2 at catalyst active sites.

The oleic acid conversion significantly increased with increasing reaction temperature and the C_{17} and C_{18} yields showed noticeable temperature dependence [16]. At a constant pressure of 60 bar, increasing hydrogenation temperature from 250 to 280 °C increased the oleic acid conversion from 87.4% to 100%. The increasing conversion with reaction temperature indicated that the HDO reaction was affected by reaction kinetics. As the temperature was increased, the oleic acid molecule gained more kinetic energy in exceeding activation energy to interact with H_2 at catalyst active sites.

The n-C_{18} selectivity was 69.4% at 250 °C, then reached a maximum (78.7%) at 280 °C and finally decreased to 64.0% at 320 °C. It is suggested that at high temperature, C_{17} and C_{18} olefins (1-olefins) possibly formed with some products of isomerization towards more stable internal alkanes via decarbonylation, deoxygenation, hydrocracking and isomerization of long chain olefins [17]. Thus, the highest catalyst activity for oleic acid HDO was achieved at temperature of 280 °C corresponding to the high n-C_{18} yield (70.3%) due to HDO reaction.

Table 1
Effects of temperature on HDO of oleic acid and palmitic acid over 0.2-$NiMoS_2$ catalyst.

Temperature (°C)	Oleic acid				Palmitic acid			
	250	280	300	320	300	320	340	360
Conversion (wt%)	87.4	100	100	100	88.4	94.2	97.7	98.9
n-alkane content (wt%)	79.6	89.4	92.5	92.5	53.6	57.1	58.6	64.3
Selectivity (wt%)								
C_{14}	–	–	–	–	1.2	1.0	1.1	1.0
C_{15}	1.4	1.2	0.9	1.1	38.5	37	41.6	48.1
C_{16}	2.3	2.0	4.2	3.7	61.6	62	57.3	50.9
C_{17}	26.9	18.1	26.0	31.2	–	–	–	–
C_{18}	69.4	78.7	68.9	64.0	–	–	–	–
Yield (wt%)								
C_{14}	–	–	–	–	0.6	0.6	0.6	0.7
C_{15}	1.1	1.1	0.8	1.0	20	21.1	24.4	30.9
C_{16}	1.8	1.8	3.9	3.4	33.0	35.4	33.6	32.7
C_{17}	21.4	16.2	24.1	28.8	–	–	–	–
C_{18}	55.3	70.3	63.7	59.3	–	–	–	–
C_{16}/C_{15}	–	–	–	–	1.7	1.7	1.4	1.1
C_{18}/C_{17}	2.6	4.3	2.6	2.1	–	–	–	–

Condition: Pressure = 60 and 30 bar for HDO of oleic acid and palmitic acid, respectively.
Catalyst weight = 0.375 wt%, oleic acid (or palmitic acid)/catalyst ratio (wt/wt) = 4.

Similarly for palmitic acid HDO at constant pressure of 30 bar, increasing temperature from 300 to 360 °C gradually increased the palmitic acid conversion from 88.4% to 98.9%. The highest catalyst activity was achieved at 320 °C, corresponding to the high n-C_{16} selectivity (62%) and n-C_{16} yield (35.4%), due to the HDO reaction. Whereas increasing temperature (280–320 °C for oleic acid HDO, 320–360 °C for palmitic acid HDO) could enhance the decarboxylation and decarbonylation reactions that the n-C_{17} selectivity (18.1–31.2%) and n-C_{17} yield (16.2–28.8%) for oleic acid HDO and n-C_{15} selectivity (37–48.1%) and n-C_{15} yield (21.1–30.9%) for palmitic acid HDO were also increased. Therefore, the oxygen removal was low at a low temperature and a low temperature favored HDO. It should be noted that the n-alkane yield of oleic acid HDO at 60 bar (79.6–92.5%) was higher than that of palmitic acid HDO at 30 bar (53.6–64.3%) indicating that pressure was the pronounced effect on HDO.

The effect of pressure on oleic acid HDO over 0.2-$NiMoS_2$ catalyst at 280 °C is presented in Table 2. When increasing initial H_2 pressure from 20 bar to 60 bar, the oleic acid conversion increased from 94% to 100%. It could be observed that the effect of increasing H_2 pressure (at 60 bar) was more pronounced on the n-C_{18} yield

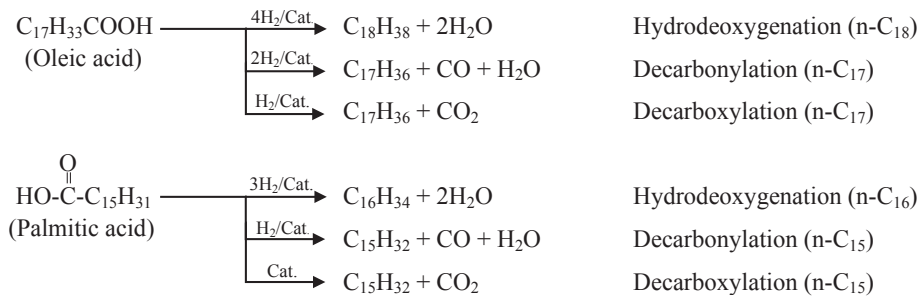

Scheme 1. Reaction scheme for HDO of oleic acid and palmitic acid on sulfide catalyst.

Table 2
Effects of pressure on HDO of oleic acid and palmitic acid over 0.2-$NiMoS_2$ catalyst.

Pressure (bar)	Oleic acid				Palmitic acid			
	20	40	60	80	30	50	70	90
Conversion (wt%)	94.2	95.1	100	100	94.2	95.1	95.2	95.4
n-alkane content (wt%)	80.9	86.3	89.4	84.8	57.1	76.0	83.6	65.7
Selectivity (wt%)								
C_{14}	–	–	–	–	1.0	0.9	0.9	1.2
C_{15}	1.9	2.5	1.2	2.2	37.0	24.4	20.6	18.4
C_{16}	5.4	5.3	2.0	3.1	62.0	74.7	78.5	80.5
C_{17}	32.1	29.3	18.1	22.2	–	–	–	–
C_{18}	60.6	62.9	78.7	72.5	–	–	–	–
Yield (wt%)								
C_{14}	–	–	–	–	0.6	0.7	0.8	0.8
C_{15}	1.5	2.1	1.1	1.9	21.1	18.6	17.2	12.1
C_{16}	4.4	4.5	1.8	2.6	35.4	56.7	65.6	52.8
C_{17}	26.0	25.4	16.2	18.8	–	–	–	–
C_{18}	49.0	54.3	70.3	61.5	–	–	–	–
C_{16}/C_{15}	–	–	–	–	1.7	3.0	3.8	4.4
C_{18}/C_{17}	1.9	2.1	4.3	3.3	–	–	–	–

Condition: Temperature = 280 °C and 320 °C for HDO of oleic acid and palmitic acid, respectively. Catalyst weight = 0.375 wt%, oleic acid (or palmitic acid)/catalyst ratio (wt/wt) = 4.

(70.3%) than on the n-C_{17} yield (16.2%). Thus, increasing H_2 pressure that was favorable for hydrogenation route, could improve the hydrogen solubility in liquid phase resulting more adsorbed hydrogen on surface of catalyst active sites as function of H_2 pressure [18].

Table 2 also shows the effect of H_2 pressure on palmitic acid HDO at 320 °C. Increasing the initial H_2 pressure from 30 to 90 bar was more pronounced on the n-C_{16} yield than the n-C_{15} yield. When H_2 pressure increased, the relative rate of decarboxylation and decarbonylation versus HDO decreased, as the latter reaction required more H_2. This study also showed that palmitic acid HDO using 0.2-$NiMoS_2$ catalysts gave a higher n-C_{16} selectivity and yield than that for n-C_{15} (C_{16}/C_{15} = 1.7–4.4), while a very low n-C_{14} selectivity and yield was obtained under all experimental conditions. Similarly, oleic acid HDO using 0.2-$NiMoS_2$ catalysts gave a higher n-C_{18} selectivity and yield than that for n-C_{17} (C_{18}/C_{17} = 1.9–4.3). Based on this study, the optimum conditions of palmitic acid HDO (320 °C and 70 bar H_2) and oleic acid HDO (280 °C and 60 bar H_2) gave a high conversion level, n-C_{16} selectivity (78.5%) and n-C_{16} yield (65.6%) and n-C_{18} selectivity (78.7%) and n-C_{18} yield (70.3%), respectively. Therefore, as the H_2 pressure increased, HDO was promoted giving a higher n-C_{16} and n-C_{18} yield for palmitic acid HDO and oleic acid HDO, respectively. In summary, a higher H_2 pressure is known to decrease the decarboxylation and favor the HDO of palmitic acid [19].

3.1.2. Effect of Ni/(Mo + Ni) and Co/(Mo + Co) atomic ratio

The effect of promoter amount (Ni or Co) on HDO of oleic acid and palmitic acid is presented in Tables 3 and 4. For oleic acid HDO using $NiMoS_2$ catalysts at Ni/(Mo + Ni) ratio of 0.1–0.4, the conversion, n-alkane content and C_{18} yield increased approaching a maximum (100%, 89.4% and 70.3%, respectively) at a Ni/(Mo + Ni) ratio of 0.2, but declined thereafter with further increasing Ni atomic ratios. Similarly for palmitic acid HDO, maximum conversion, n-alkane content and C_{16} yield (95.5%, 83.6% and 65.6%, respectively) was obtained at Ni/(Mo + Ni) ratio of 0.2.

Moreover, for oleic acid HDO and palmitic acid HDO using $CoMoS_2$ catalysts at Co/(Mo + Co) ratio of 0.1–0.4, the conversion, n-alkane content and C_{18} and C_{16} yields increased approaching a maximum (Co/(Mo + Co) ratio of 0.2 for oleic acid HDO and 0.3 for palmitic acid HDO) but declined thereafter with further increasing Co atomic ratios.

Table 3
Effects of Ni/(Mo + Ni) mole ratio on HDO of oleic acid and palmitic acid over unsupported sulfide catalysts.

Ni/(Mo + Ni)	Oleic acid					Palmitic acid				
	0.1	0.2	0.3	0.4	1	0.1	0.2	0.3	0.4	1
Conversion (wt%)	95.1	100	97.2	93.8	88.0	93.0	95.2	94.2	88.2	82.8
n-alkane content (wt%)	91.1	89.4	82.8	85.9	12.6	64.0	83.6	58.8	37.6	4.4
Selectivity (wt%)										
C_{14}	–	–	–	–	–	1.1	0.9	1.2	1.7	16.7
C_{15}	1.3	1.2	1.8	1.7	0.0	29.2	20.6	27.7	32.2	54.4
C_{16}	3.0	2.0	0.9	1.1	6.3	69.7	78.5	71.1	66.1	28.9
C_{17}	20.7	18.1	24.3	28.9	54.6	–	–	–	–	–
C_{18}	75.0	78.7	73.0	68.3	39.1	–	–	–	–	–
Yield (wt%)										
C_{14}	–	–	–	–	–	0.7	0.8	0.7	0.7	0.7
C_{15}	1.2	1.1	1.5	1.5	0.0	18.7	17.2	16.3	12.1	2.4
C_{16}	2.7	1.8	0.8	1.0	0.8	44.6	65.6	41.8	24.8	1.3
C_{17}	18.9	16.2	20.0	24.8	6.9	–	–	–	–	–
C_{18}	68.3	70.3	60.1	58.6	4.9	–	–	–	–	–
C_{16}/C_{15}	–	–	–	–	–	2.4	3.8	2.6	2.0	0.5
C_{18}/C_{17}	3.6	4.3	3.0	2.4	0.7	–	–	–	–	–

Condition: Temperature = 280 °C, Pressure = 60 bar for oleic acid HDO.
Temperature = 320 °C, Pressure = 70 bar for palmitic acid HDO.
Catalyst weight = 0.375 wt%, oleic acid (or palmitic acid)/catalyst ratio (wt/wt) = 4.

Table 4
Effects of Co/(Mo + Co) mole ratio on HDO of oleic acid and palmitic acid over unsupported sulfide catalyst.

Co/(Mo + Co)	Oleic acid					Palmitic acid				
	0.1	0.2	0.3	0.4	1	0.1	0.2	0.3	0.4	1
Conversion (wt%)	87.2	96.1	94.8	91.9	88.4	86.8	84.4	90.1	83.0	82.4
n-alkane content (wt%)	33.5	60.0	34.8	29.1	8.1	43.7	31.6	49.3	26.4	6.2
Selectivity (wt%)										
C_{14}	–	–	–	–	–	1.8	2.3	1.8	2.5	9.4
C_{15}	2.9	1.5	5.3	5.2	7.3	20.0	27.9	19.7	28.0	66.6
C_{16}	3.6	7.5	11.6	4.8	8.6	78.3	69.7	78.6	69.5	23.9
C_{17}	30.1	21.4	26.4	25.5	65.5	–	–	–	–	–
C_{18}	63.4	69.6	56.7	64.5	18.6	–	–	–	–	–
Yield (wt%)										
C_{14}	–	–	–	–	–	0.8	0.7	0.9	0.7	0.6
C_{15}	1.0	0.9	1.9	1.5	0.6	8.7	8.8	9.7	7.4	4.1
C_{16}	1.2	4.5	4.0	1.4	0.7	34.2	22.1	38.7	18.3	1.5
C_{17}	10.1	12.8	9.2	7.2	5.3	–	–	–	–	–
C_{18}	21.2	41.8	19.7	18.8	1.5	–	–	–	–	–
C_{16}/C_{15}	–	–	–	–	–	3.9	2.5	4.0	2.5	0.4
C_{18}/C_{17}	2.1	3.3	2.1	2.6	0.3	–	–	–	–	–

Condition: Temperature = 280 °C, Pressure = 60 bar for oleic acid HDO.
Temperature = 320 °C, Pressure = 70 bar for palmitic acid HDO.
Catalyst weight = 0.375 wt%, oleic acid (or palmitic acid)/catalyst ratio (wt/wt) = 4.

The MoS_2 catalyst activity was enhanced after Ni or Co addition whereas the opposite trend of surface area was reported (section 3.2). Thus, the hydrogenation activity of the MoS_2 catalyst was not correlated to the surface area but rather more strongly depended on the morphology. The increased hydrogenation efficiency was due to that more active sites were formed at low Ni or Co concentration in Mo sulfide catalyst. As increasing Ni/(Mo + Ni) atomic ratio above 0.2 or Co/(Mo + Co) above 0.3, the conversion, n-alkane content, C_{16} and C_{18} yields decreased drastically due to the bulk formation of the Ni or Co promoter that partially covered the active promoted Mo sites [20,21].

3.2. Catalysts characterization

In the catalyst synthesis, the bimetallic (Ni-Mo or Co-Mo) sulfide precursor is generated by the chemical reaction of Ni or Co

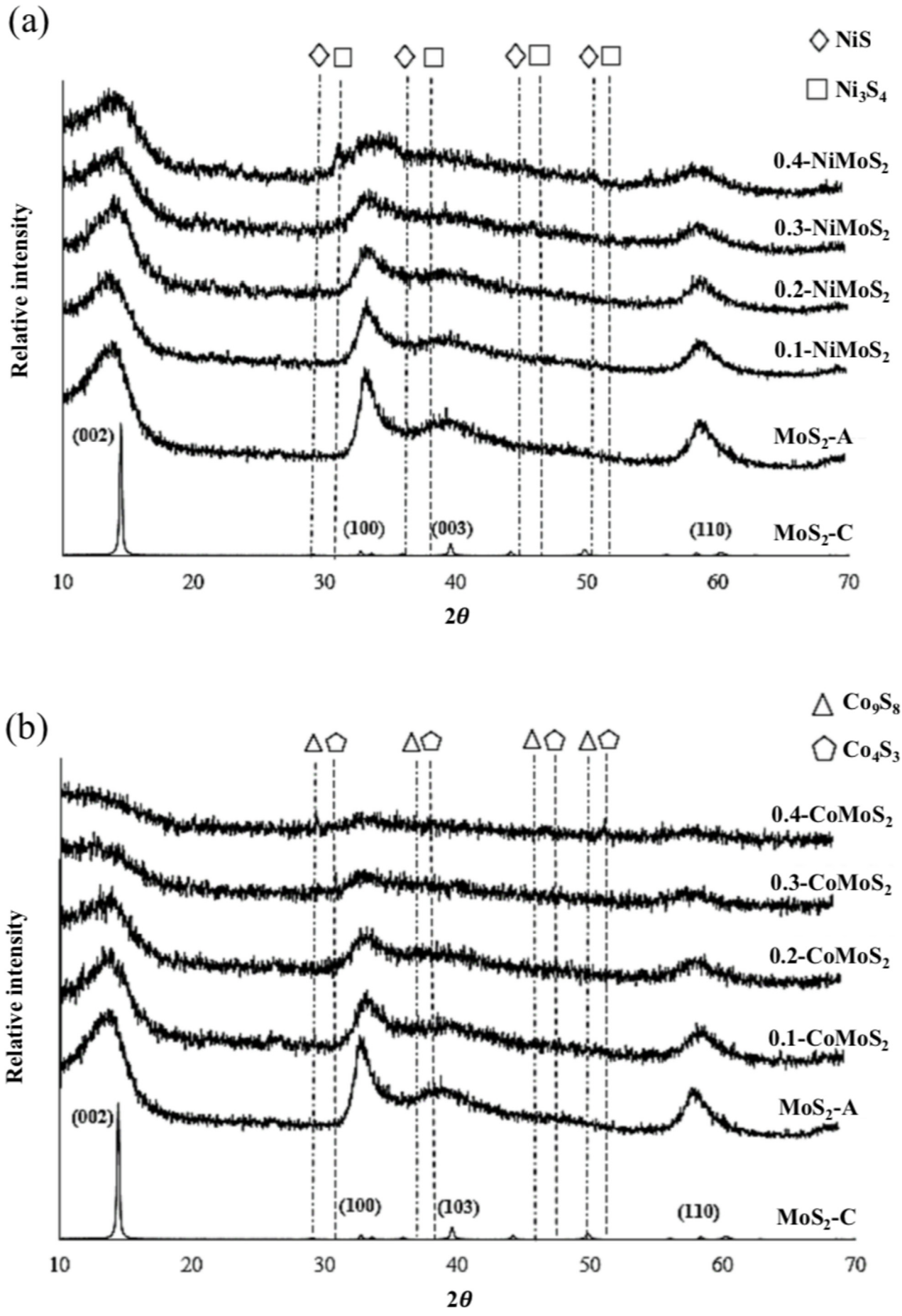

Fig. 1. XRD patterns of MoS_2-C, MoS_2-A, (a) unsupported Ni-Mo sulfide catalysts with various Ni/(Mo + Ni) atomic ratios and (b) unsupported Co-Mo sulfide catalysts with various Co/(Mo + Co) atomic ratios.

precursor ($Ni(NO_3)_2$ or $Co(NO_3)_2$) and ATTM solution as suggested in Eq. (1). After that, $Ni(MoS_4)_2$ is transformed to $Ni(MoS_2)_2$ with the removal of sulfur in the excess hydrogen atmosphere as shown in Eqs. (2) and (3) which Me is Ni or Co [22]:

$$2(NH_4)_2MoS_4 + Me(NO_3)_2 \rightarrow (NH_4)_2\{Me(MoS_4)_2\} + 2NH_4NO_3 \quad (1)$$

$$Me\ (MoS_4)_2 + H_2 \rightarrow Me(MoS_3)_2 + H_2S \quad (2)$$

$$Me(MoS_3)_2 + H_2 \rightarrow Me(MoS_2)_2 + H_2S \quad (3)$$

From this preparation, a highly dispersion of Ni or Co atoms on nano-crystallite Mo sulfide is expected since, during the hydrothermal decomposition in the presence of H_2, Mo is surrounded by Ni or Co in the solution. This well dispersion is necessary for the development of a number of Ni-Mo-S or Co-Mo-S structure which has been known as the most active site for hydrogenation reaction.

Fig. 1 shows the XRD patterns of the Mo sulfide and Ni-Mo sulfide catalysts ($NiMoS_2$). While the crystallite MoS_2 (MoS_2-C) showed a sharp narrowing peak in the pattern of a highly crystallized MoS_2 structure, the peak characteristics of the amorphous MoS_2-A were broad and overlapping corresponding to an amorphous triclinic MoS_2-like phase indicating a highly disordered packing of the MoS_2 layer. This conclusion would be supported by the transmission electron microscopy (TEM) analysis which the TEM micrographs of these catalysts show the MoS_2 crystallites in the pattern of parallel dark line groups (Fig. 2).

The MoS_2 slabs in the catalyst can be presented as parallel dark line and the spacing between these MoS_2 slabs is about 0.65 nm which correspond to the (0 0 2) basal planes of crystalline MoS_2. From the TEM micrographs, the MoS_2-A from the hydrothermal preparation had a folded multi-layered structure with bending, whereas MoS_2-C presented a stack with straight multi-layered pattern. This shows a characteristic of a crystalline structure confirmed by XRD results (Fig. 1). The slab length of the MoS_2-A was about 15 nm, which is over two-fold smaller than that of MoS_2-C (33 nm), while the average number of layers in the stacks of MoS_2-A (2–7 layers) was lower than that of MoS_2-C (10 layers) (Table 5).

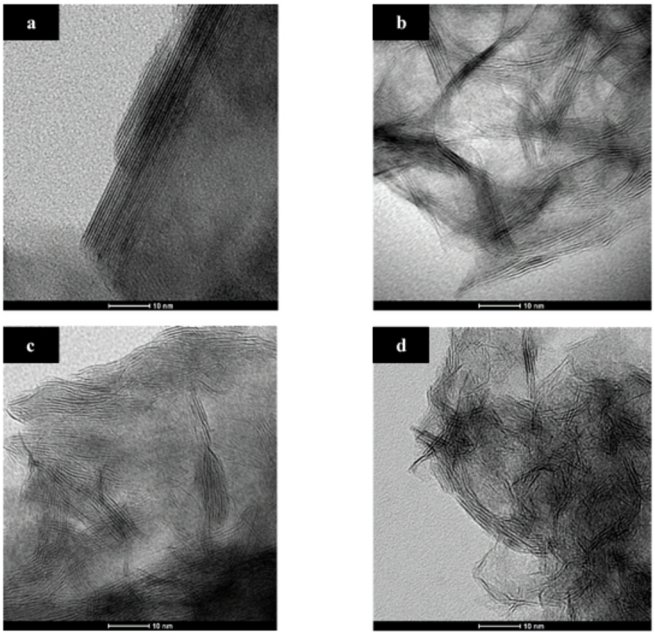

Fig. 2. TEM images of (a) MoS_2-C, (b) MoS_2-A, (c) 0.2-$NiMoS_2$ and (d) 0.2- $CoMoS_2$ catalysts.

Table 5
Physical properties of MoS_2-C, MoS_2-A, 0.2-$NiMoS_2$ and 0.2-$CoMoS_2$.

Catalysts	Slab length (nm)	Number of stacks	Number of layers
MoS_2-C	33	1	10
MoS_2-A	15	8	2–7
0.2-$NiMoS_2$	10	9	5–7
0.2-$CoMoS_2$	8	11	2–5

The distinguished XRD results and TEM micrographs implied that there is a difference in structural and morphological properties of MoS_2-A and MoS_2-C catalysts.

For the amorphous $NiMoS_2$ and $CoMoS_2$ catalyst, the intensity of the sharp XRD peaks was reduced to almost absence, specifically for the peak at $2\theta = 14.4$, characteristic of the (0 0 2) basal planes of crystalline MoS_2. Thus, the formation of a much smaller size of the (0 0 2) phase of MoS_2 confirm the incorporation of Ni promoter into the MoS_2 structure particularly on the (0 0 2) phase. For the $NiMoS_2$ catalysts at Ni/(Mo + Ni) ratio above 0.2 (Fig. 1a), the diffraction peaks of the second metal sulfide appeared progressively, and Ni_3S_4 and NiS were detected in the catalysts. In most cases, the ternary Mo-Ni-S phase did not appeared clearly due to that there was overlapping of diffraction peaks from MoS_2 and Mo-Ni-S phase. Eventually, the $NiMoS_2$ and $CoMoS_2$ catalysts showed the diffraction peaks of poorly crystalline MoS_2, indicating that the MoS_2 maintained its structure in the presence of amorphous Ni or Co [22,23]. In the same manner, the catalysts with the Co/(Mo + Co) ratio above 0.2 (Fig. 1b), Co_9S_8 and Co_4S_3 were detected in the catalysts. For the promoted sulfide catalysts, the Ni–Mo–S or Co–Mo–S phases possibly presented as small nano-sized particles, which could not be detected by XRD method.

This crystalline structure observed by XRD analysis would also be supported by the TEM analysis (Fig. 2). From the TEM micrograph of the 0.2-$NiMoS_2$ and 0.2-$CoMoS_2$, MoS_2 crystallites in the pattern of parallel dark line group could be seen (Fig. 2c and d). The parallel dark line as the MoS_2 slabs with spacing are characteristics of the (0 0 2) basal planes of crystalline MoS_2. Hence, the hydrothermal method gave the MoS_2 with long slab, and with the Ni promoter incorporation, the slabs with more curvature became shorter, indicating the small particle formation. The decrease of number of layers in the stacks was also observed (Table 5). The increase in stacking affected the HDO activity of catalyst. From TEM observation, the rim sites of MoS_2 slabs containing metallic states presumably involved in hydrogenation and the stacking of the MoS_2 increased the number of exposed rim sites leading to higher the hydrogenation [24]. The decreasing slab length in the TEM analysis (Table 5) showed a good agreement with the XRD results indicating that the shorter size of (0 0 2) basal planes of MoS_2 was formed in $NiMoS_2$ and $CoMoS_2$catalyst. The contradiction is that the Ni or Co addition obstructed the development of MoS_2 crystallized particles. This causes the smaller crystallized structure compared with the MoS_2.

Table 6 and Fig. 3 present the effect of promoter amount (Ni or Co) on the sulfide catalysts in terms of the BET specific surface area, pore volume and the N_2 adsorption-desorption isotherms, respectively. The hydrothermal preparation led to Mo-S catalyst with amorphous structure. This prepared catalyst presents a high surface area of 204.3 m^2/g and pore volume of 0.33 cm^3/g. However, the surface area of Mo sulfide catalysts can be in the range of 50–300 m^2/g depending on the precursor and synthesis condition [25,26]. Here, the higher amount of Ni promoter caused the reduction of BET surface area and pore volume in bimetallic sulfide catalysts [27,28] and the 0.4-$NiMoS_2$ had the less surface area and pore volume. From the N_2 adsorption-desorption isotherms (Fig. 3), all MoS_2, $NiMoS_2$ and $CoMoS_2$ catalysts showed type IV isotherms

Table 6
Composition and properties of MoS_2-C, MoS_2-A, $NiMoS_2$-A and $CoMoS_2$-A unsupported catalysts with various Ni/(Mo + Ni) or Co/(Mo + Co) atomic ratios.

Catalysts	Ni/(Mo + Ni) or Co/(Mo + Co)	Surface area (m^2/g)	Pore volume (cm^3/g)
MoS_2-C	0.0	11.9	0.20
MoS_2-A	0.0	204.3	0.33
0.1-$NiMoS_2$	0.1	116.1	0.18
0.2-$NiMoS_2$	0.2	123.6	0.18
0.3-$NiMoS_2$	0.3	100.5	0.11
0.4-$NiMoS_2$	0.4	46.6	0.07
0.1-$CoMoS_2$	0.1	106.0	0.15
0.2-$CoMoS_2$	0.2	123.1	0.19
0.3-$CoMoS_2$	0.3	81.1	0.10
0.4-$CoMoS_2$	0.4	25.9	0.04

with a hysteresis loop characteristic of mesoporous particles [22,29].

For the amorphous MoS_2, $NiMoS_2$ and $CoMoS_2$ catalysts, the TPR profiles (Fig. 4) showed two separated strong peaks at low and high temperatures. At the low temperature region, the weakly bonded sulfur on the surface was reduced. This TPR peak appears to be directly related to the formation of active sites by the elimination of non-stoichiometric sulfur, in other words the highly labile sulfur present at the edges or corners of the MoS_2 crystallites. Thus, the coordinative unsaturated sites (CUS) were created, which are believed to be responsible for the observed catalytic activity [30]. At the high temperature region, the "bulk reduction" occurred. The TPR profiles also illustrated that the peak maxima/minima position

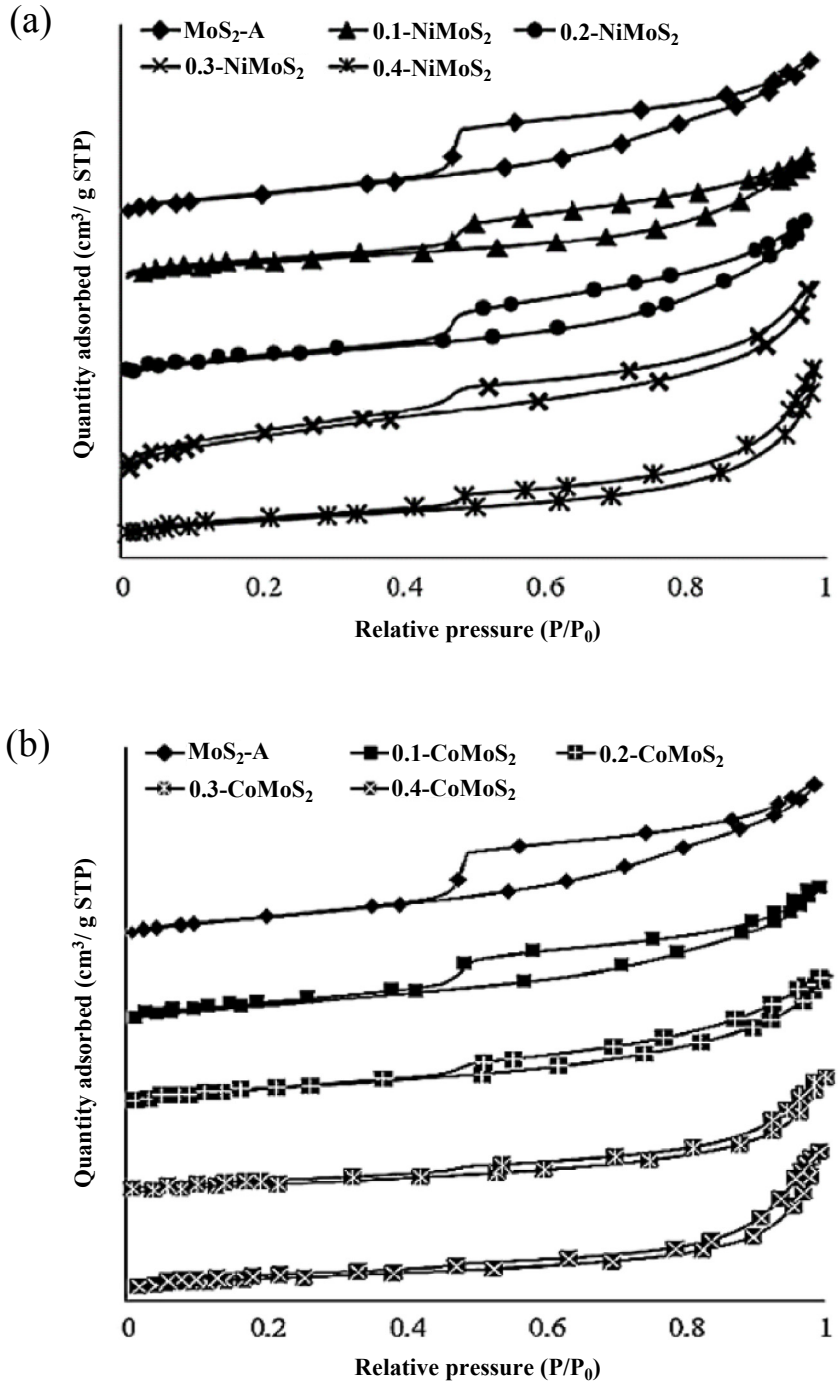

Fig. 3. N_2 adsorption/desorption isotherms of (a) Ni–Mo and (b) Co-Mo sulfides with various Ni/(Mo + Ni) or Co/(Mo + Co) atomic ratios.

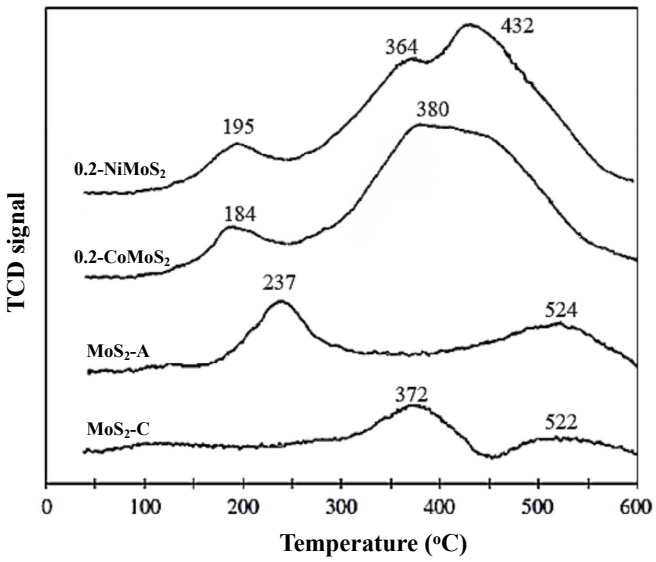

Fig. 4. TPR profiles of MoS_2-C, MoS_2-A, 0.2-$NiMoS_2$ and 0.2-$CoMoS_2$ catalysts.

depended on the structure and promoter of the MoS_2 catalyst [23]. The MoS_2-A catalyst had the two main peaks at 237 and 524 °C, whereas MoS_2-C had the low temperature zone peak was at 372 °C. This TPR data presents a lower sulfur bond energy of MoS_2-A as compared to MoS_2-C. It implies that the Mo-S bond strength in MoS_2-A is weaker than that of MoS_2-C.

The TPR experiments also revealed that the position of the TPR peak is sensitive to the presence of the promoters (Co and Ni). For Co or Ni promoted Mo sulfide catalysts, the first peak was found at lower temperature. The 0.2-$NiMoS_2$ catalyst had broad peaks at reduction temperatures of 195 and 364 °C and 0.2-$CoMoS_2$ at 180 and 380 °C. This result shows that the sulfur – metal bond energy at the edges of Co(Ni)MoS is weaker than the one at the edges of MoS_2-A. Thus, the sulfur atom could be eliminated easily in a promoted catalyst, leading to the creation of sulfur vacancies (CUS) present on the edges of the MoS_2 slabs.

3.3. Catalytic activity of oleic acid and palmitic acid HDO

The crystalline MoS_2, amorphous MoS_2, $NiMoS_2$ and $CoMoS_2$ catalyst activity is also compared in terms of oleic acid and palmitic acid conversion, product selectivity and product yield (Table 7). For sulfide catalysts, the proposed mechanism of carboxylic acid hydrogenation consisting three pathways involves direct C=O bonds scission (direct HDO) yielding n-C_{16} and n-C_{18} products, and also via decarboxylation and decarbonylation leading to n-C_{15} and n-C_{17} products.

From Table 7, the palmitic acid and oleic acid conversion from HDO using the 0.2-Ni–MoS_2 and MoS_2-A catalysts was higher than that using MoS_2-C. For the products of oleic acid HDO over the different MoS_2 catalysts, n-C_{17} and n-C_{18} yields varied in their relative proportions (yield) that C_{18}/C_{17} ratio from HDO using the 0.2-$NiMoS_2$ (4.3) and MoS_2-A catalyst (2.7) that was higher than that using MoS_2-C (2.3). Similarly, C_{16}/C_{15} ratio from palmitic HDO using the 0.2-$NiMoS_2$ (3.8) and MoS_2-A catalyst (2.4) was higher than that using MoS_2-C (1.6). The n-C_{16} and n-C_{18} which is formed via the direct HDO reaction, was preferentially formed by MoS_2-A compared with MoS_2-C, while n-C_{15} and n-C_{17} which are produced by the combined decarboxylation and decarbonylation reactions, was mostly formed by MoS_2-C compared with MoS_2-A.

The catalyst activity was ranked (in terms of n-alkane content, C_{18} and C_{16} yields) in decreasing order as:

For oleic acid HDO (C_{18} yield): 0.2-$NiMoS_2$ > 0.3-$CoMoS_2$ ~ MoS_2-A > MoS_2-C

For palmitic acid HDO (C_{16} yield): 0.2-$NiMoS_2$ > 0.3-$CoMoS_2$ > MoS_2-A > MoS_2-C

The 0.2-NiMo sulfide catalyst exhibited better performance than 0.3-CoMo sulfide for oleic acid and palmetic acid HDO. The increased rate of the oleic acid and palmitic acid HDO was due to the high catalytic activity of MoS_2 catalyst that was enhanced by the Ni promoter addition. For the $NiMoS_2$ catalyst, the decreased BET surface area and pore volume were compensated by a decreased slab length and an increased curvature of the MoS_2 slabs which Ni located on the edge of the MoS_2 structure could prevent the crystallite aggregation.

Table 7
Comparison of sulfide catalyst on HDO of oleic acid and palmitic acid.

Catalyst	Oleic acid					Palmitic acid				
	No catalyst	MoS_2-C	MoS_2-A	0.2-$NiMoS_2$	0.2-$CoMoS_2$	No catalyst	MoS_2-C	MoS_2-A	0.2-$NiMoS_2$	0.3-$CoMoS_2$
Conversion (%)	78.9	84.6	91.9	100.0	96.1	76.9	79.1	82.8	95.2	90.1
n-alkane content (wt%)	5.6	57.0	59.9	89.4	60.0	4.7	26.9	30.4	83.6	49.3
Selectivity (%)										
C_{14}	–	–	–	–	–	0.0	3.1	2.3	0.9	1.8
C_{15}	0.0	0.0	0.8	1.2	1.5	55.5	37.1	28.6	20.6	19.7
C_{16}	0.0	9.1	7.2	2.0	7.5	44.5	59.8	69.1	78.5	78.6
C_{17}	51.7	27.6	24.8	18.1	21.4	–	–	–	–	–
C_{18}	48.3	63.3	67.2	78.7	69.6	–	–	–	–	–
Yield (wt%)										
C_{14}	–	–	–	–	–	0.0	0.8	0.7	0.8	0.9
C_{15}	0.0	0.0	0.5	1.1	0.9	2.6	10.0	8.7	17.2	9.7
C_{16}	0.0	5.2	4.3	1.8	4.5	2.1	16.1	21.0	65.6	38.7
C_{17}	2.9	15.7	14.9	16.2	12.8	–	–	–	–	–
C_{18}	2.7	36.1	40.2	70.3	41.8	–	–	–	–	–
C_{16}/C_{15}	–	–	–	–	–	0.8	1.6	2.4	3.8	4.0
C_{18}/C_{17}	0.9	2.3	2.7	4.3	3.3	–	–	–	–	–

Condition: Temperature = 280 °C, Pressure = 60 bar for oleic acid HDO.
Temperature = 320 °C, Pressure = 70 bar for palmitic acid HDO.
Catalyst weight = 0.375 wt%, oleic acid (or palmitic acid)/catalyst ratio (wt/wt) = 4.

These unsupported catalysts with some Ni content compared to conventional supported catalysts have an increased catalytic activity that supported by the added Ni promoters present as Ni sulfide, as suggested by the XRD analysis. The Ni promoted MoS_2 catalyst showed higher activity due to the decreased strength of the Mo–S–Ni bond in the Mo sulfide catalyst also supported by a significant shift to the lower reduction temperature suggested by TPR analysis. Beside the scientific point of view on the efficient $NiMoS_2$ catalyst, the results on reaction conditions and n-C_{15}, n-C_{16}, n-C_{17} and n-C_{18} yields of HDO are beneficial to the vegetable oil (containing oleic acid and palmitic acid) evaluation and the process design for biodiesel production.

4. Conclusion

The hydrogenation of oleic acid and palmitic acid over unsupported Ni-Mo and Co-Mo sulfide catalysts prepared by the hydrothermal method was studied to find the appropriate conditions and catalyst. For oleic acid HDO at optimal condition (280 °C and 60 bar H_2), the Ni-Mo sulfide catalysts (Ni/(Ni + Mo) = 0.2) had shown better performance than Co-Mo sulfide in terms of oleic acid conversion (100%), n-C_{18} selectivity (78.8%) and n-C_{18} yield (70.3%). For palmitic acid HDO at optimum condition (320 °C and 70 bar H_2), the Ni-Mo sulfide catalyst (Ni/(Ni + Mo) = 0.2) also gave the highest n-C_{16} selectivity and n-C_{16} yield. This implied that the Ni-Mo sulfide catalyst promoted the HDO reaction rather than decarboxylation and decarbonylation reactions. High pressure favored HDO pathway, while high temperature strongly affected the decarboxylation and decarbonylation pathways. It can be also concluded that HDO is the catalytic process while decarboxylation and decarbonylation are thermal and catalytic process.

Acknowledgements

The funding support, equipments and all materials provided by the National Metal and Materials Technology Center (MTEC), National Science and Technology Development Agency are gratefully acknowledged (P-17-50647).

References

[1] A. Guzman, J.E. Torres, L.P. Prada, M.L. Nuñez, Hydroprocessing of crude palm oil at pilot plant scale, Catal. Today 156 (2010) 38–43.
[2] L. Hermida, A.Z. Abdullah, A.R. Mohamed, Deoxygenation of fatty acid to produce diesel-like hydrocarbons: a review of process conditions, reaction kinetics and mechanism, Renew. Sustain. Energy Rev. 42 (2015) 1223–1233.
[3] S. Mikkonen, Second-generation renewable diesel offers advantages, Hydrocarb. Process. 19 (2008) 63–66.
[4] S. Izhar, H. Kanesugi, H. Tominaga, M. Nagai, Cobalt molybdenum carbides: surface properties and reactivity for methane decomposition, Appl. Catal. A Gen. 317 (2007) 82–90.
[5] V. Sundaramurthy, A.K. Dalai, J. Adjaye, Comparison of P-containing γ-Al_2O_3 supported Ni-Mo bimetallic carbide, nitride and sulfide catalysts for HDN and HDS of gas oils derived from Athabasca bitumen, Appl. Catal A Gen. 311 (2006) 155–163.
[6] B. Diaz, S.J. Sawhill, D.H. Bale, R. Main, D.C. Phillips, S. Korlann, et al., Hydrodesulfurization over supported monometallic, bimetallic and promoted carbide and nitride catalysts, Catal. Today 86 (2003) 191–209.
[7] B. Veriansyah, J.Y. Han, S.K. Kim, S.-A. Hong, Y.J. Kim, J.S. Lim, et al., Production of renewable diesel for hydroprocessing of soybean oil: effect of catalysts, Fuel 94 (2012) 578–585.
[8] M. Krar, S. Kovacs, D. Kallo, J. Hancsok, Fuel purpose hydrotreating of sunflower oil on CoMo/Al_2O_3 catalyst, Bioresour. Technol. 101 (2010) 9287–9293.
[9] A. Srifa, K. Faungnawakij, V. Itthibenchapong, N. Viriya-empikul, T. Charinpanitkul, S. Assabumrungrat, Production of bio-hydrogenated diesel by catalytic hydrotreating of palm oil over $NiMoS_2$/Al_2O_3 catalyst, Bioresour. Technol. 158 (2014) 81–91.
[10] I. Sebos, A. Matsoukas, V. Apostolopoulos, N. Papayannakos, Catalytic hydroprocessing of cottonseed oil in petroleum diesel mixtures for production of renewable diesel, Fuel 88 (2009) 145–149.
[11] M. Toba, Y. Abe, H. Kuramochi, M. Osako, T. Mochizuki, Y. Yoshimura, Hydrodeoxygenation of waste vegetable oil over sulfide catalysts, Catal. Today 164 (2011) 533–537.
[12] S. Eijsbouts, S.W. Mayo, K. Fujita, Unsupported transition metal sulfide catalysts : from fundamentals to industrial application, Appl Catal A Gen 322 (2007) 58–66.
[13] B. Yoosuk, C. Song, J.H. Kim, C. Ngamcharussrivichai, P. Prasassarakich, Effects of preparation conditions in hydrothermal synthesis of highly active unsupported NiMo sulfide catalysts for simultaneous hydrodesulfurization of dibenzothiophene and 4,6-dimethyldibenzothiophene, Catal. Today 149 (2010) 52–61.
[14] M. Ameen, M.T. Azizan, S. Yusup, A. Ramli, M. Yasir, Catalytic hydrodeoxygenation of triglycerides: an approach to clean diesel fuel production, Renew. Sustain. Energy Rev. 80 (2017) 1072–1088.
[15] B. Yoosuk, J.H. Kim, C.S. Song, C. Ngamcharussrivichai, P. Prasassarakich, Highly active MoS_2, $CoMoS_2$ and $NiMoS_2$ unsupported catalysts prepared by hydrothermal synthesis for hydrodesulfurization of 4,6-dimethyldibenzothiophene, Catal. Today 130 (2008) 14–23.
[16] D. Kubička, L. Kaluža, Deoxygenation of vegetable oils over sulfided Ni, Mo and NiMo catalysts, Appl. Catal. A Gen. 372 (2010) 199–208.
[17] A.E. Couman, E.J.M. Hensen, A model compound (methyl oleate, oleic acid, triolein) study of triglyceride hydrodeoxygenation over alumina-supported Ni-Mo sulfide, Appl. Catal. B Environ. 201 (2017) 290–301.
[18] W. Wang, L. Li, K. Wu, K. Zhang, J. Jie, Y. Yang, Preparation of Ni-Mo-S catalysts by hydrothermal method and their hydrodeoxygenation properties, Appl. Catal. A Gen. 495 (2015) 8–16.
[19] Y. Yang, Q. Wang, X. Zhang, L. Wang, G. Li, Hydrotreating of C_{18} fatty acids to hydrocarbons on sulphided NiW/SiO_2-Al_2O_3, Fuel Process. Technol. 116 (2013) 165–174.
[20] P. Gajardo, A. Mathieux, P. Grange, B. Delmon, Structure and catalytic activity of CoMo/γ-Al_2O_3 and CoMo/SiO_2 hydrodesulphurization catalysts: an XPS and ESR characterization of sulfided used catalysts, Appl. Catal. 3 (1982) 347–376.
[21] O.İ. Şenol, T.-R. Viljava, A.O.I. Krause, Hydrodeoxygenation of methyl esters on sulphided NiMo/γ-Al_2O_3 and CoMo/γ-Al_2O_3 catalysts, Catal. Today 100 (2005) 331–335.
[22] B. Yoosuk, D. Tumnanthong, P. Prasassarakich, Amorphous unsupported Ni-Mo sulfide prepared by one step hydrothermal method for phenol hydrodeoxygenation, Fuel 91 (2012) 246–252.
[23] B. Yoosuk, D. Tumnanthong, P. Prasassarakich, Unsupported MoS_2 and $CoMoS_2$ catalysts for hydrodeoxygenation of phenol, Chem. Eng. Sci. 79 (2012) 1–7.
[24] M. Daage, R.R. Chianelli, Structure-function relations in molybdenum sulfide catalysts: the “Rim-Edge” model, J. Catal. 149 (1994) 414–427.
[25] G. Alonso, G. Berhault, A. Aguilar, V. Collins, C. Ornelas, S. Fuentes, R.R. Chianelli, Characterization and HDS activity of mesoporous MoS_2 catalysts prepared by in situ activation of tetraalkylammonium thiomolybdates, J. Catal. 208 (2002) 359–369.
[26] M.H. Siadati, G. Alonso, B. Torres, R.R. Chianelli, Open flow hot isostatic pressing assisted synthesis of unsupported MoS_2 catalysts, Appl. Catal. A Gen. 305 (2006) 160–168.
[27] F. Pedraza, S. Fuentes, Ni–Mo and Ni–W sulfide catalysts prepared by decomposition of binary thiometallates, Catal. Lett. 65 (2000) 107–113.
[28] N. Escalona, J. Ojeda, P. Baeza, R. Garcia, J.M. Palacios, J.L.G. Fierro, et al., Synergism between unsupported Re and Co or Ni sulfide catalysts in the HDS and HDN of gas oil, Appl. Catal. A Gen. 287 (2005) 47–53.
[29] K.S.W. Sing, D.H. Everett, R.A.W. Haul, L. Moscou, R.A. Pierotti, J. Rouquerol, et al., Reporting physisorption data for gas solid systems with special reference to the determination of surface area and porosity, Pure Appl. Chem. 57 (1985) 603–619.
[30] P. Afanasiev, On the interpretation of temperature programmed reduction patterns of transition metals sulfides, Appl. Catal. A Gen 303 (2006) 110–115.